pp. 1–14 (2015)

Viscous dissipation energy as a risk factor in multiple cerebral aneurysms

A. K. Khe*,† A. P. Chupakhin* , A. A. Cherevko* , Sh. Sh. Eliava‡ and Yu. V. Pilipenko‡

Abstract — The hydrodynamic properties of the blood flow in cerebral vessels with multiple aneurysms are studied in the paper. We compare the sets of parameters derived from the dissipation energy appearing due to the blood viscosity and computed for different aneurysms of one patient. Numerical simulations show that in most cases the dissipation energy and its derived parameters are lower in the case of ruptured aneurysm. Moreover, the average dissipation energy per unit volume is lower in all cases studied here.

Keywords: Hemodynamics, dissipation energy, multiple aneurysms, mathematical modelling, numerical simulation.
MSC 2010: 76Z05, 76D05, 65-04

A cerebral aneurysm is a local enlargement of the arterial wall caused by wall damage and weakening. In most cases aneurysms occur at the places of anatomic variations and pathological conditions or high-flow arteriovenous malformations which cause locally increased flows in the cerebral circulation and at points of flow bifurcations [14]. The arterial aneurysm is one of the most frequent and dangerous diseases of cerebral arteries. The most serious consequences of the presence of an aneurysm are its rupture and intracranial hemorrhage which could be lethal. According to statistics, up to 5% of all deceased people being in autopsy have cerebral aneurysms. The treatment of aneurysms is a challenging task because often there are no visible symptoms of aneurysms before their rupture. At the same time, a treatment carries a risk of complications which can exceed the risk of the aneurysm's rupture on early stage. Thus, at the moment when a neurosurgeon recognizes that a patient has an aneurysm, he meets a problem of determining the time when it is better to treat the patient. To start surgery in time, a surgeon must know how the aneurysm is growing and when (and if) the risk of its rupture exceeds the critical value.

*Lavrentyev Institute of Hydrodynamics, Lavrentyev prospect, 15, Novosibirsk 630090, Russia. Corresponding author: alekhe@hydro.nsc.ru

†Novosibirsk State University, Novosibirsk 630090, Russia

‡Burdenko Research Institute of Neurosurgery, 4th Tverskaya-Yamskaya, 16, Moscow 125047, Russia

The theoretical research of this paper was supported by the Russian Foundation for Basic Research (project No. 14-01-00036). The blood vessel segmentation, 3D reconstruction from CT scans, and numerical simulations were supported by the Russian Science Foundation (project No. 14-35-00020).

Despite an arterial aneurysm is a rather frequent disease and the study of aneurysms is a very urgent subject, the mechanisms of its formation, growth, evolution, and rupture are not well understood yet. There are several factors involved in those processes such as histological, hemodynamic, and genetic ones. A lot of papers are focused on assessment of these factors. Systematic reviews and meta-analysis of the prevalence and the risk of rupture of intracranial aneurysms based on the studies up to 2011 can be found in [13, 16]. The estimates are based on 1,450 unruptured intracranial aneurysms of 94,912 patients.

The study of morphological parameters in the context of aneurysm rupture in the presence of multiple aneurysms was reported in [6]. The analysis revealed a number of parameters dependent on the geometry of the aneurysm that can be considered as significant when comparing multiple aneurysms of one patient. The aspect ratio, size ratio, parent-daughter angle are among them. In [10], based on the study of 134 patients with 294 aneurysms, the authors concluded that the age, size, and site of the aneurysm should be taken into account. Moreover, it was found that the rate of aneurysm rupture in the anterior communicating artery is significantly higher. Morphological and hemodynamical factors of rupture of multiple unilateral aneurysms on the anterior circulation were studied in [21]. A geometrical analysis showed that ruptured aneurysms have irregular shape and significantly higher maximum heights and aspect ratios. The hemodynamics of ruptured aneurysms was characterized by a lower minimum wall shear stress (WSS) and a larger low-WSS area.

The existence of such a large number of factors makes the treatment planning quite a challenging problem for a neurosurgeon. The risk of intra- and post-operative complications brings up a question of immediate surgery. To measure the risk associated with the treatment and to improve the management of the unruptured intracranial aneurysms, the natural history and clinical outcome were studied in [18]. The authors note that the age of a patient is a strong predictor of surgical outcome. The results of a long-term follow-up study of factors affecting the formation and growth of aneurysms were presented in [8]. The authors had found that the rupture of an aneurysm is very much related to its growth. Among several potential risk factors tested, only the cigarette smoking and female sex were, after adjustment for age, significant independent risk factors for occurrence and growth of an aneurysm.

Mathematical modelling of multiple intracranial aneurysms is a more challenging problem than that of a single aneurysm. In the case of multiple aneurysms, the domain of examination is several times larger, which increases the segmentation time and computational costs. The questions to answer here are the following: do the aneurysms influence each other, what is the best treatment plan, in what order should the aneurysms be operated, or is it better to operate them all at once? There are few papers on this subject. We point out recent paper [7] where the hemodynamics of small aneurysm pairs at the internal carotid artery was studied. The authors considered four aneurysm pair cases with each pair at the supraclinoid segment of the internal carotid artery. Their results had shown that the relative anatomic location of one aneurysm with respect to the other one may determine the hemodynamic environment of the aneurysm.

Thus, a mathematical modelling based on patient-specific clinical data can greatly help in finding possible predictors of aneurysm rupture. In this paper we demonstrate an application of one such parameter of several available hydrodynamic and mechanical ones. In our previous papers [17, 19] we studied local characteristics of the blood flow in the presence of a single aneurysm (both hydrodynamic and mechanical parameters). In this paper we study hydrodynamic properties in the case of multiple aneurysms. Our key ingredient for this research is the dissipation energy appearing due to the viscosity of the blood. We compare the sets of parameters derived from it for different aneurysms of one patient.

The structure of the paper is as follows. In Section 1 we formulate the mathematical model used here to describe the blood flow in cerebral vessels with aneurysms. The description of study cases is presented in Section 2. We specify the numerical tool box used for simulation and introduce the dissipation energy parameter used for comparisons. The results obtained and discussion can be found in Section 3. The conclusion is formulated in Section 4.

1. Mathematical modelling

Modelling such complex and multifactorial objects, one always has to find a balance between a mathematical model describing the phenomenon most accurately, but being computationally very expensive, and a simpler one, but describing only basic features of the case.

In order to describe the blood flow in a vessel lumen, we use the Navier–Stokes equations governing non-stationary three dimensional flows of an incompressible viscous Newtonian fluid, i.e.,

$$\operatorname{div}\mathbf{v} = 0, \quad \rho\big(\mathbf{v}_t + (\mathbf{v}\cdot\nabla)\mathbf{v}\big) + \nabla p = \mu\Delta\mathbf{v}, \quad \mathbf{x}\in\Omega,\ t\in(0,T) \tag{1.1}$$

where $\mathbf{v}$ is the velocity vector, ρ is the constant density, p is the pressure, and μ is the dynamic viscosity. The flow domain Ω is a fixed domain in $\mathbb{R}^3$ representing the reconstructed vessel lumen.

The boundary conditions for equations (1.1) are the following. No-slip condition must hold on the vessel wall $\partial\Omega_{\text{wall}}$, i.e.,

$$\mathbf{v} = 0, \quad \mathbf{x}\in\partial\Omega_{\text{wall}},\ t\in(0,T).$$

At the inlets $\partial\Omega_{\text{in}}$ of the domain we specify the normal velocity

$$\mathbf{v} = v_{\text{in}}(t)\,\mathbf{n}, \quad \mathbf{x}\in\partial\Omega_{\text{in}},\ t\in(0,T)$$

while at the outlets $\partial\Omega_{\text{out}}$ of the domain we prescribe the given pressure

$$p = p_{\text{out}}(t), \quad \mathbf{x}\in\partial\Omega_{\text{out}},\ t\in(0,T).$$

Numerical simulations are performed starting from the initial conditions at rest, namely,

$$\mathbf{v}|_{t=0} = 0, \quad p|_{t=0} = p_{\text{ref}}, \quad \mathbf{x}\in\Omega.$$

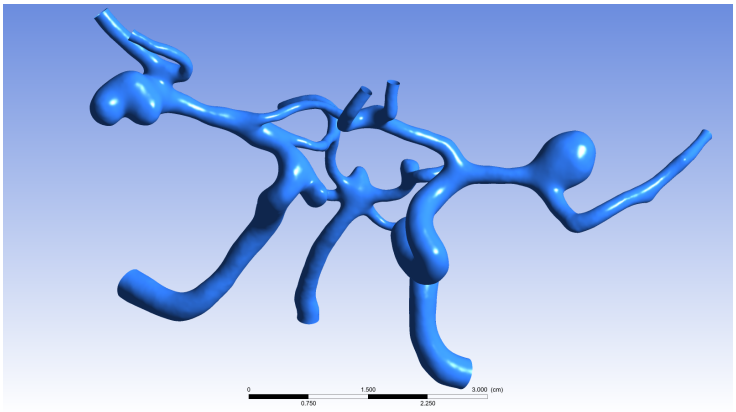

Figure 1. Multiple (six) aneurysms in the cerebral arterial circulation.

The reference pressure p_{ref} is the atmospheric pressure of 760 mm Hg.

The blood itself is considered as an incompressible fluid with the density of 997 kg/m^3 and the dynamic viscosity of 0.004 Pa·s.

We note that the uniform velocity profile specified at the inlets does not significantly change the flow in the aneurysms. Indeed, the entrance length is proportional to the Reynolds number Re and the diameter of the vessel D and is approximately determined by the expression $L = 0.03\,\mathrm{Re}\,D$ [2, 9]. In our case we have

$$D \approx 3 \text{ mm}, \qquad |\mathbf{v}| \approx 0.6 \text{ m/s}, \qquad \mathrm{Re} = \rho|\mathbf{v}|D/\mu \approx 449.$$

Thus, the entrance length is approximately equal to $L \approx 4$ cm, which is sufficient in our cases. In our previous paper [19] we showed that extending the inlet boundaries in order to develop the velocity profile completely, the outcome is not significantly changed.

2. Materials and methods

In this paper we apply a patient specific non-stationary numerical 3D simulations of relatively large cerebral arterial circulation areas with multiple aneurysms (Fig. 1). The patients were treated at the Burdenko Research Institute of Neurosurgery. We studied five cases with the diagnoses shown in Table 1. The patients suffered hemorrhages at locations indicated by exclamation marks.

The simulations use CT scans obtained in the preoperative examinations. The reconstruction of flow domains from the tomography images was performed with the ITK-SNAP segmentation procedure [20] and the *Vascular Modeling Toolkit* [1] software. The reconstructed domains are shown in Fig. 2.

There were no measurements of blood flow velocity carried out for these patients during their treatment. Instead of using an arbitrary periodic function for boundary conditions (e.g., trigonometric functions or their linear combinations), we set up the velocity $v_{\text{in}}(t)$ and the pressure $p_{\text{out}}(t)$ time dependencies at the boundaries to clinical data, but measured for different patients with cerebral aneurysm.

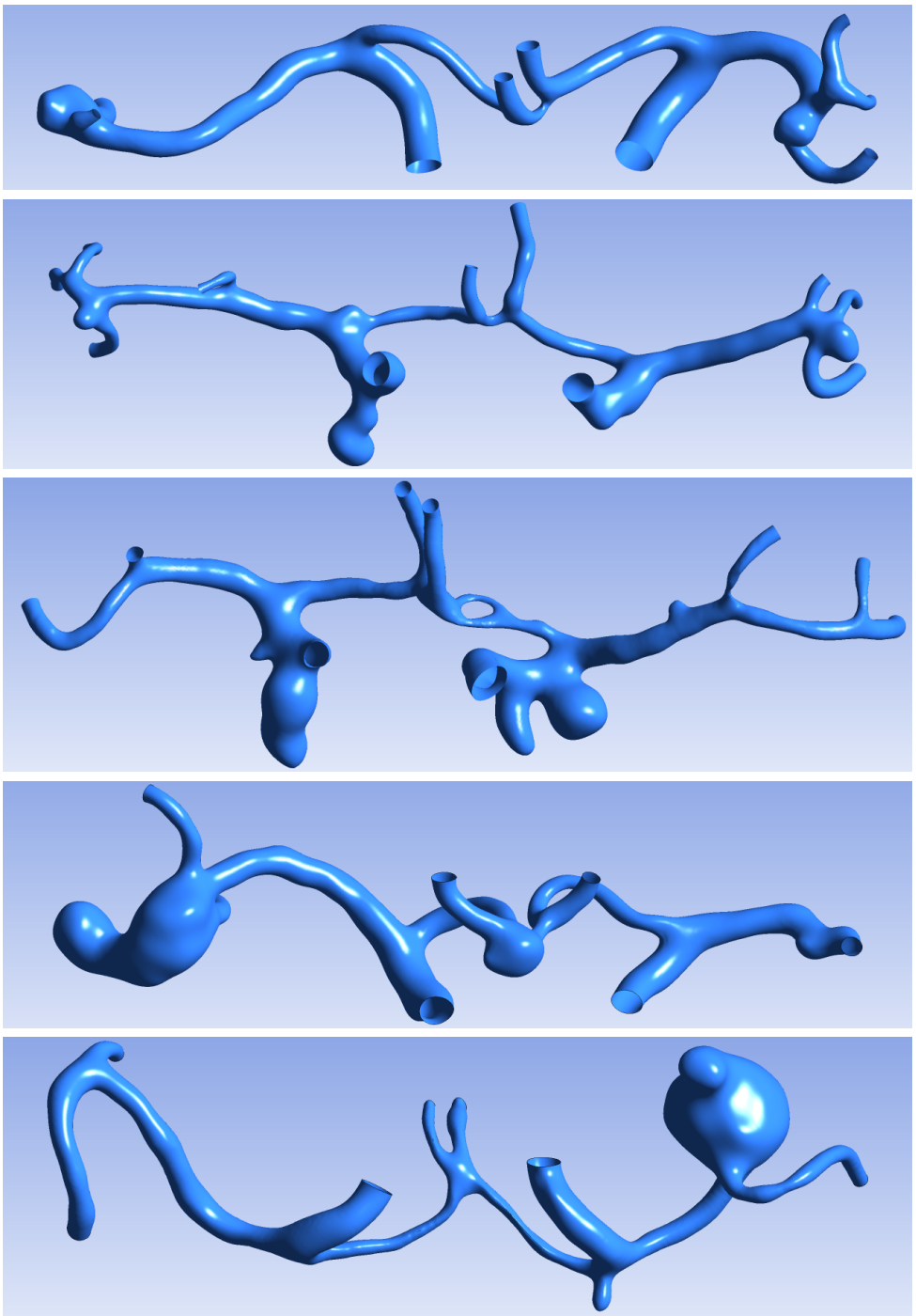

Figure 2. Computational domains of cerebral vessels with multiple aneurysms for the patients ANB, SLS, BEP, LYE, DRZ (from top to bottom).

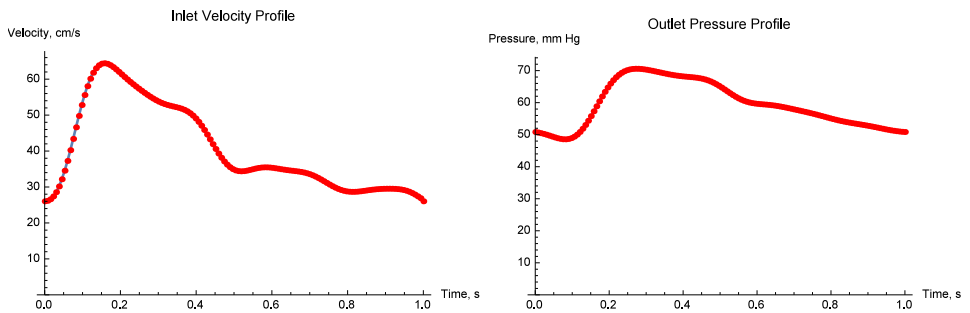

Figure 3. Velocity at the inlet and pressure at the outlet measured in an endovascular surgery of cerebral arterial aneurysm (one period).

Table 1.
Cases studied. The exclamation mark denotes the location of the hemorrhage.

Patient	Sex, age	Diagnosis
ANB	F, 54	2 aneurysms: left MCA (!), right MCA
SLS	F, 56	3 aneurysms: right supraclinoid segment (!), right MCA, left MCA and aneurysmal protrusion of left ICA
BEP	F, 53	4 aneurysms: communicating segment of right ICA (!), choroid segment of right ICA, and 2 supraclinoid segment of left ICA
LYE	M, 55	2 aneurysms: bifurcation of right MCA (!), right ACA-ACommA region
DRZ	M, 54	2 aneurysms: bifurcation of left MCA, bifurcation of left ICA (!)

Such choice of boundary conditions allows us to avoid the need to construct artificial physiological velocity and pressure profiles.

At the inlets and outlets of the flow domain we use the blood flow parameters (velocity and pressure) taken from intraoperative monitoring with Volcano ComboMap endovascular blood flow measurement system [4]. The ComboMap system uses Volcano ComboWire guide wire with pressure and ultrasound transducers. The guide wire is 0.36 mm in diameter and has the working length of 185 cm. The measurements were carried out in the Meshalkin Novosibirsk Research Institute of Circulation Pathology during the endovascular treatment of cerebral arterial aneurysms. Typical profiles without any singularities and obtained in a low-noise measurement session were taken for boundary conditions. One-heart-beat data were scaled to a one-second time interval and extended periodically. The velocity and pressure profiles used for boundary conditions are shown in Fig. 3.

Numerical computations were performed for a 3-second time interval and the last one-second interval $t \in [2,3]$ was taken for the periodic solution.

Numerical computations were carried out in the Informational and Computational Centre of the Novosibirsk State University using ANSYS commercial software. Hydrodynamic properties of the flow were calculated using the ANSYS CFX solver.

The numerical scheme used in the CFX solver is based on the modified SIMPLE (Semi-Implicit Method for Pressure Linked Equations) scheme [22]. The solver

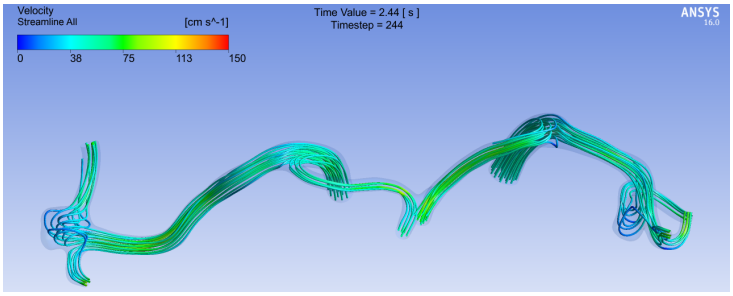

Figure 4. Stream lines of the velocity vector field for patient ANB.

uses a finite volume method for spatial discretization of the Navier–Stokes equations (1.1) and the second order backward Euler scheme for the transient term. The resulting scheme is implicit, conservative, and has no time step limitations. The pressure–velocity coupling is based on the discretizations described in [11, 12] where a method avoiding the decoupling of the pressure field was proposed. This approach results in a coupled solver solving the Navier–Stokes equations as a single system with a completely implicit discretization scheme.

The results of our simulations are in agreement with the common view on the physiological flows in cerebral arteries. As an example, we present velocity stream lines in Fig. 4 (patient ANB). A detailed analysis of hydrodynamic flows in vessels with aneurysms is the subject of many papers [14] including our works [17, 19]. In this paper we use a set of variables derived from principal hydrodynamic ones.

In a flow of viscous incompressible fluid, the total mechanical energy dissipating in a unit time interval depends on the vortex intensity inside the domain [15]:

$$W = 4\mu \int_{\Omega} |\omega|^2 \, \mathrm{d}\Omega \tag{2.1}$$

where W is the dissipation energy per unit time interval, μ is the dynamic viscosity, and $\omega = \nabla \times \mathbf{v}$ is the vortex vector. For each case considered here, we isolate the subdomains corresponding to the aneurysms and calculate the energy dissipating in these subdomains.

Our main goal is to compare the energies dissipating in the aneurysmal sacs of one patient.

3. Results and discussion

Each aneurysmal sac was selected manually using a spherical boundary with the centre at the fundus of the aneurysm. The cutting sphere was chosen so that its intersection with the flow domain boundary closely corresponds to the aneurysm neck. The regions of the aneurysms at the bifurcations of the right and left middle cerebral arteries of the patient ANB are shown in Fig. 5.

The surface of the flow domain boundary inside the sphere is considered as the wall of the aneurysm (the dome of the aneurysm).

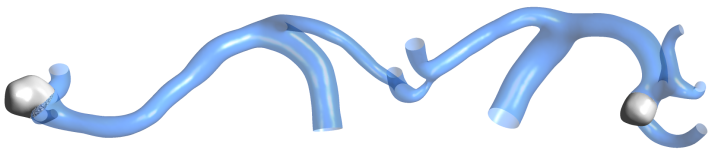

Figure 5. Subdomains of the flow corresponding to the aneurysmal sacs.

Table 2.
Volumes and surface areas of the aneurysm.

Patient	Aneurysm	Volume, mm^3	Area, mm^2
ANB	left MCA (!)	26.26	34.05
	right MCA	62.47	65.33
SLS	right ICA (!)	69.12	93.77
	right MCA	8.57	16.74
	left MCA	30.07	40.33
BEP	right ICA (!)	127.56	131.61
	left ICA #1	43.51	60.11
	left ICA #2	94.89	95.49
LYE	right MCA (!)	416.67	332.24
	ACommA	56.78	59.73
DRZ	left MCA (!)	1,504.12	671.33
	bif. left ICA	14.58	28.58

Table 3.
Total dissipation energy and dissipation energy per unit surface area.

Patient	Aneurysm	W_{max}, mW	E, mJ	$\bar{E}$, kJ/m^3	$W_{s\,max}$, W/m^2	E_s, J/m^2
ANB	left MCA (!)	0.15	0.06	2.28	4.26	1.78
	right MCA	0.40	0.18	2.88	6.11	2.77
SLS	right ICA (!)	0.45	0.16	2.31	4.77	1.76
	right MCA	0.53	0.24	28.00	31.76	14.06
	left MCA	0.68	0.27	8.98	16.81	6.77
BEP	right ICA (!)	0.03	0.01	0.08	0.26	0.11
	left ICA #1	0.14	0.06	1.38	2.27	0.99
	left ICA #2	0.15	0.06	0.63	1.52	0.64
LYE	right MCA (!)	0.28	0.12	0.29	0.85	0.36
	ACommA	0.15	0.07	1.23	2.23	0.97
DRZ	left MCA (!)	1.52	0.72	0.48	2.27	1.08
	bif. left ICA	0.05	0.02	1.37	1.84	0.76

The calculated volumes and surface areas of the aneurysms are summarized for the cases studied here in Table 2. It is worth noting that in most cases (4 of 5) the rupture followed by a subarachnoid hemorrhage occurs in the largest aneurysm.

Along with the dissipation energy rate W, we introduce the following quantities describing different energy characteristics of the flow:

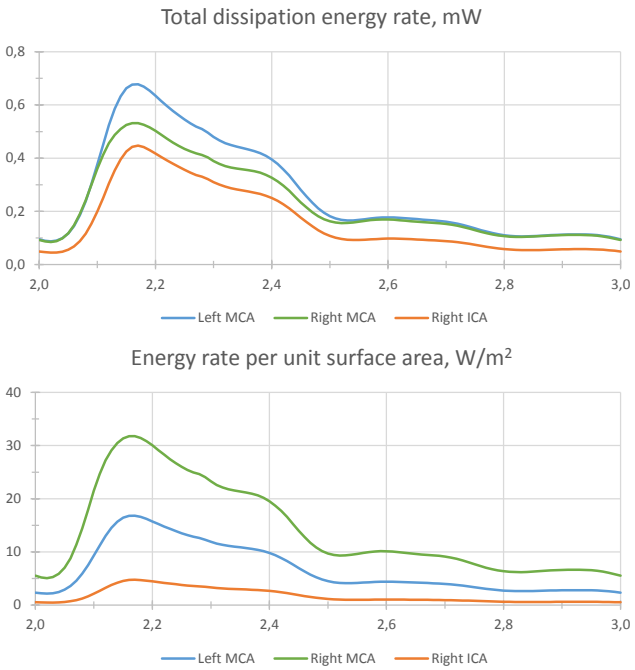

Figure 6. Total dissipation energy rate and dissipation energy rate per surface area for patient SLS.

— the total dissipation energy per one period (i.e. one heart beat) $E = \int_0^T W \, \mathrm{d}t$;

— the average dissipation energy per unit volume $\bar{E} = E/V$;

— the dissipation energy rate per unit surface area $W_{\mathrm{s}} = W/S$;

— the total dissipation energy per unit surface area $E_{\mathrm{s}} = E/S$.

The calculation results of the dissipating energy are shown in Table 3. In column 3, maximal dissipation energy rate (2.1), $W_{\max} = \max_t W$, is shown for each aneurysm. Column 6 contains the maximal dissipation energy rate per unit surface area of the aneurysm over the time period, $W_{\mathrm{s}\,\max} = \max_t W_{\mathrm{s}}$.

The total dissipation energy rate and the dissipation energy per surface area for patient SLS over the period are shown in Fig. 6.

Our simulations show that in 3 cases out of 5 the dissipation energy rate and the total energy over one period are less for ruptured aneurysms. In these three cases the volume of the aneurysms is less compared to the other two cases.

Considering the specific energy per unit surface area, in 4 cases out of 5 we obtain a lesser value for ruptured aneurysms. We note also that for patients SLS and BEP the values of the energy and specific energy for unruptured aneurysms are switched over.

In contrast to other parameters, the average dissipation energy $\bar{E}$ in all five cases turns out to be the least for the ruptured aneurysms.

The results obtained here agree in some sense with those of [21] and [7] where

it was shown that the wall shear stress in the ruptured aneurysms is lower and the low WSS area is larger.

The results obtained imply the conjecture that a lower dissipation energy might be considered as a potential marker of possible rupture of the aneurysm. Such possibility may be justified with the following explanation. The energy of flow dissipation appearing due to viscosity is the energy absorbed by the surrounding media, i.e., in our case, by the vessel walls. The energy loss may occur in the fluid flow due to a heat transfer or smaller scale motion. In our simulations we assumed that the flow régime corresponds to a 'steady-state', non-acute, non-critical patient's conditions. This means that the aneurysm has already developed and we study the properties of the blood flow at this very moment (leaving its growth and formation off the model). Under these assumptions, the blood flow transfers dissipation energy to the vessel walls and the walls getting less energy are less 'stimulated' and hence less 'strengthened'. These weaker walls developed under normal conditions are more prone to rupture if abnormal conditions such as abrupt pressure or flow rate increase occur. Thus, the energy dissipating in the aneurysmal sac can affect the integrity of the vessel wall and cause its rupture.

3.1. Non-Newtonian models

Since the blood is not homogeneous fluid and contains a lot of formed elements, its viscosity is determined by several parameters such as plasma viscosity, hematocrit, mechanical properties of red blood cells [2]. In this section we study the dependence of the viscous dissipation energy on rheological properties of the blood.

For our simulations we employ four constitutive models used in [5] where effects of non-Newtonian behavior on the hemodynamics of cerebral aneurysms were studied. Those are the Herschel–Bulkley, Casson, and two Carreau–Yasuda models. The models are defined by the following relations between the dynamic viscosity μ and the shear strain rate $\dot{\gamma}$.

The Herschel–Bulkley model. This is the model for viscoplastic fluids that, after yield, exhibits a power law behavior in shear stress versus shear strain rate, i.e.,

$$\mu = \frac{\tau_y}{\lambda\dot{\gamma}} + K(\lambda\dot{\gamma})^{n-1}$$

with the yield stress $\tau_y = 0.0175$ Pa, the viscosity consistency $K = 8.9721$ mPa·s, the time constant $\lambda = 1$ s, and the power law index $n = 0.8601$.

The Casson model. This model is a variation of the Bingham model for viscoplastic fluids with the following square root/quadratic dependency:

$$\sqrt{\mu} = \sqrt{\frac{\tau_y}{\dot{\gamma}}} + \sqrt{K}$$

with the yield stress $\tau_y = 0.015625$ Pa and the viscosity consistency $K = 0.0052$ Pa·s.

Table 4.
Total dissipation energy in the left and right MCA aneurysms in patient ANB.

Model	E_{left}, mW	E_{right}, mW	Diff., left, %	Diff., right, %
Newtonian	6.06	18.07		
Herschel–Bulkley	5.87	16.99	−3.1	−6.0
Casson	5.37	17.58	−11.4	−2.7
Carreau–Yasuda A	6.05	17.63	−0.2	−2.5
Carreau–Yasuda B	5.75	16.54	−5.2	−8.5

The Carreau–Yasuda model (A and B). This is a generalization of Carreau's original model

$$\mu = \mu_\infty + \frac{\mu_0 - \mu_\infty}{\left(1 + (\lambda\dot{\gamma})^a\right)^{(1-n)/a}}$$

with the low shear viscosities $\mu_0 = 0.056$ Pa·s, the high shear viscosities $\mu_\infty = 0.00345$ Pa·s, the time constant $\lambda = 1.902$ s, the power law index $n = 0.22$, and the Yasuda exponent $a = 1.25$ for model A; and $\mu_0 = 0.022$ Pa·s, $\mu_\infty = 0.0022$ Pa·s, $\lambda = 0.110$ s, $n = 0.392$, and $a = 0.644$ for model B.

The results of simulations based on these constitutive models for patient ANB are shown in Figs. 7 and 8. In Fig. 7 the dissipation energy rate in the aneurysms at the left and right MCA are presented. The graphs clearly show a qualitative and quantitative concordance of the energy rate over the time period. The relative differences between the energy rates calculated by the non-Newtonian constitutive models and the Newtonian one, $(W_{\text{nonNewton}} - W_{\text{Newton}})/W_{\text{Newton}}$, are shown in Fig. 8. In almost all the cases (except for the Casson model) the non-Newtonian rheology decreases the dissipation energy rate by up to 10% uniformly over time. We note that the decrease values for different rheology models correspond to each other between the left and right aneurysms. This means that the inequality between the energy rates (and the derived variables) in the left and the right aneurysms remains the same when switching from the Newtonian model to a non-Newtonian one.

In the case of Casson's model the distinction between the relative differences of the dissipation rates in the left and the right aneurysms is more essential (about 10%). However, the distribution of the energy rate differences over the time period is the same for the left and right domains. This means that the application of Casson's model changes the dissipation rate over time in the same way for both flow domains. The inequality may be violated if the difference between the rates for the left and the right aneurysms is less than 10%. In the latter case the difference is probably insignificant for any conclusion on the question whether the dissipation energy can predict the rupture of the aneurysm.

The total viscous dissipation energy over one time period is shown in Table 4. The results conform to the expected relation between the values for the left and the right flow domains (i.e., it is the same as in the Newtonian model). The relative changes are up to 11% with the maximal value for Casson's model. We note that in

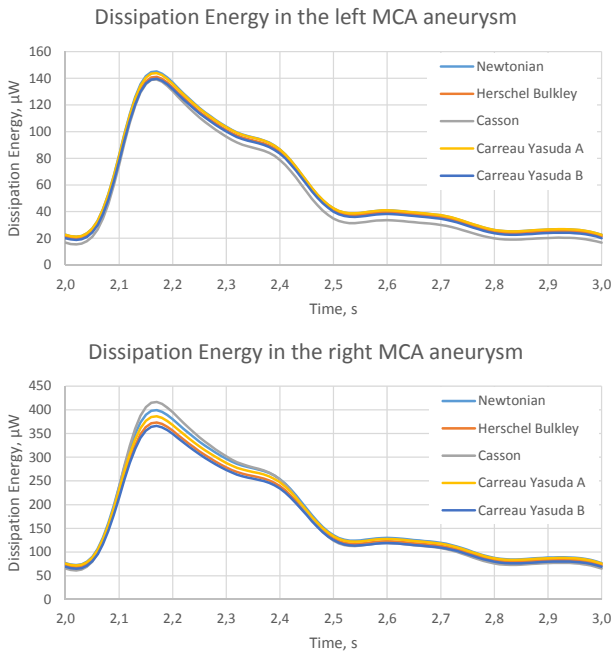

Figure 7. Dissipation energy rate computed by the non-Newtonian models of blood for patient ANB.

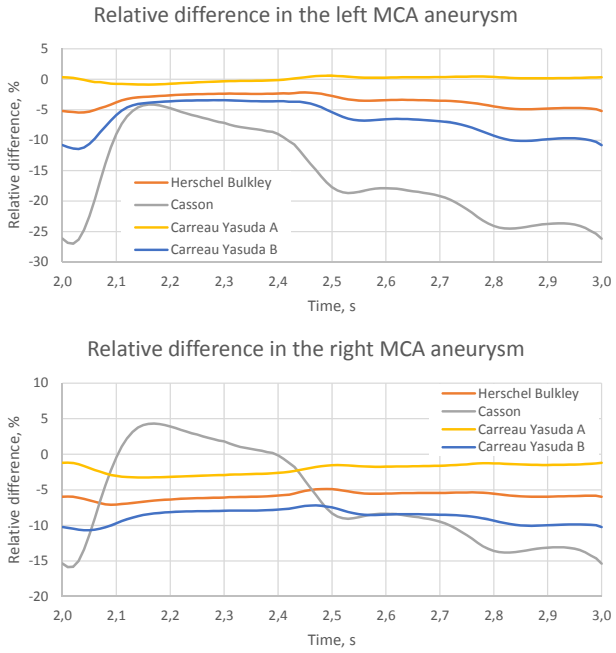

Figure 8. Difference of the dissipation energy rate computed by the non-Newtonian models relative to the Newtonian model for patient ANB.

most cases (except for the Casson model) the decrease of the total energy is larger in the domains with higher total energy.

Thus, the application of non-Newtonian models for studying viscous dissipation energy properties in multiple aneurysms does not reveal any significant differences in the outcome compared to the results obtained with the Newtonian model.

4. Conclusion

Mathematical modelling of the hemodynamics of the cerebral circulatory system in its full formulation is a rather complex FSI problem [3]. In our experience of patient-specific simulations of hemodynamics of the cerebral aneurysms, numerical computations under the full formulation of FSI problems (with coupled ANSYS CFX and ANSYS Mechanical solvers) cost more than 80 times higher than computations under the rigid-wall assumption (almost 1 week against 2 hours on a 6-core processor). The goal of our research is to find the parameters that could indicate a higher risk of one aneurysm rupture compared to the others in the multiple aneurysm case. Such predictors should be relatively 'cheap' computationally in order to provide calculations in the preoperative examination. Therefore, we focus our attention exclusively on the hydrodynamic part of the flow.

Five cases of multiple intracranial aneurysms were considered. Numerical simulations showed that in most cases the viscous dissipation energy and its derived parameters are lower in a ruptured aneurysm. Moreover, the average dissipation energy per unit volume in the ruptured aneurysm is lower in all cases studied here. The use of a non-Newtonian blood rheology does not show any essential distinctions in the results. Thus, this quantity might be considered as a significant parameter in treatment planning for patients with multiple aneurysms.

References

1. L. Antiga and D. Steinman, *The Vascular Modeling Toolkit*. URL:http://www.vmtk.org/.
2. O. K. Baskurt, R. Hardeman, and W. Rampling, *Handbook of Hemorheology and Hemodynamics*. IOS Press, Amsterdam, 2007.
3. Y. Bazilevs, K. Takizawa, and T. E. Tezduyar, *Computational Fluid-Structure Interaction: Methods and Applications*. Wiley Series in Computational Mechanics, Wiley, 2013.
4. A. P. Chupakhin, A. A. Cherevko, A. K. Khe, N. Yu. Telegina, A. L. Krivoshapkin, K. Yu. Orlov, V. A. Panarin, and V. I. Baranov, Measurement and analysis of cerebral hemodynamic parameters in the presence of brain vascular anomalies. *Circul. Pathol. Cardiac Surgery* **4** (2012), 27–31.
5. C. Fisher and J. S. Rossmann, Effect of non-newtonian behavior on hemodynamics of cerebral aneurysms. *J. Biomech. Engrg.* **131** (2009), No. 9, 091004.
6. H. J. Jeon, J. W. Lee, S. Kim, K. Y. Park, and S. K. Huh Morphological parameters related to ruptured aneurysm in the patient with multiple cerebral aneurysms (clinical investigation). *Neurol. Research* **36** (2014), No. 12, 1056–1062.

7. L.-D. Jou, H. Morsi, H. M. Shaltoni, and M. E. Mawad, Hemodynamics of small aneurysm pairs at the internal carotid artery. *Medical Engrg. Physics* **34** (2012), No. 10, 1454–1461.

8. S. Juvela, K. Poussa, and M. Porras, Factors affecting formation and growth of intracranial aneurysms: a long-term follow-up study. *Stroke* **32** (2001), 485–491.

9. W. M. Kays and M. E. Crawford, *Convective Heat and Mass Transfer*, McGraw-Hill, 1993.

10. H.-T. Lu, H.-Q. Tan, B.-X. Gu, W. Wang, and M.-H. Li, Risk factors for multiple intracranial aneurysms rupture: a retrospective study. *Clinical Neurol. Neurosurgery* **115** (2013), No. 6, 690–694.

11. S. Majumdar, Role of underrelaxation in momentum interpolation for calculation of flow with nonstaggered grids. *Numer. Heat Transfer* **13** (1988), No. 1, 125-132.

12. C. M. Rhie and W. L. Chow, *A numerical study of the turbulent flow past an isolated airfoil with trailing edge separation*. In: 3rd Joint Thermophysics, Fluids, Plasma and Heat Transfer Conference, AIAA Paper 82-0998, (1982).

13. G. J. E. Rinkel, M. Djibuti, A. Algra, and J. van Gijn, Prevalence and risk of rupture of intracranial aneurysms: a systematic review. *Stroke* **29** (1998), 251–256.

14. D. M. Sforza, C. M. Putman, and J. R. Cebral, Hemodynamics of cerebral aneurysms. *Annual Review Fluid Mech.* **41** (2009), 91–107.

15. N. A. Slyozkin, *Dynamics of Viscous Incompressible Fluid*. GITTL, Moscow, 1955 (in Russian).

16. M. H. M. Vlak, A. Algra, R. Brandenburg, and G. J. E. Rinkel, Prevalence of unruptured intracranial aneurysms, with emphasis on sex, age, comorbidity, country, and time period: a systematic review and meta-analysis. *The Lancet Neurology* **10** (2011), No. 7, 626–636.

17. N. A. Vorobtsova, A. A. Yanchenko, A. A. Cherevko, A. P. Chupakhin, A. L. Krivoshapkin, K. Yu. Orlov, V. A. Panarin, and V. I. Baranov, Modelling of cerebral aneurysm parameters under stent installation. *Russ. J. Numer. Anal. Math. Modelling*, **28** (2013), No. 5, 505–516.

18. D. O. Wiebers, Unruptured intracranial aneurysms: natural history, clinical outcome, and risks of surgical and endovascular treatment. *The Lancet* **362** (2003), No. 9378, 103–110.

19. A. A. Yanchenko, A. A. Cherevko, A. P. Chupakhin, A. L. Krivoshapkin, and K. Yu. Orlov, Nonstationary hemodynamics modelling in a cerebral aneurysm of a blood vessel. *Russ. J. Numer. Anal. Math. Modelling* **29** (2014), No. 5, 307–317.

20. P. A. Yushkevich, J. Piven, H. C. Hazlett, R. G. Smith, S. Ho, J. C. Gee, and G. Gerig, User-guided 3D active contour segmentation of anatomical structures: Significantly improved efficiency and reliability. *NeuroImage* **31** (2006), No. 3, 1116–1128.

21. Y. Zhang, X. Yang, Y. Wang, J. Liu, C. Li, L. Jing, S. Wang, and H. Li, Influence of morphology and hemodynamic factors on rupture of multiple intracranial aneurysms: matched-pairs of ruptured-unruptured aneurysms located unilaterally on the anterior circulation. *BMC Neurology* **14** (2014), 253.

22. *ANSYS Documentation. ANSYS CFX Theory Guide*. ANSYS, Inc., URL:http://www.ansys.com/.